Hindawi Publishing Corporation
Journal of Chemistry
Volume 2015, Article ID 608265, 8 pages
http://dx.doi.org/10.1155/2015/608265

*Research Article*

# Evaluation of Optimal Pore Size of (3-Aminopropyl)triethoxysilane Grafted MCM-41 for Improved $CO_2$ Adsorption

**Zhilin Liu, Yang Teng, and Kai Zhang**

*Beijing Key Laboratory of Emission Surveillance and Control for Thermal Power Generation, North China Electric Power University, Beijing 102206, China*

Correspondence should be addressed to Kai Zhang; kzhang@ncepu.edu.cn

Received 3 June 2015; Revised 27 July 2015; Accepted 30 July 2015

Academic Editor: Khaldoun Bachari



An array of new MCM-41 with substantially larger average pore diameters was synthesized through adding 1,3,5-trimethylbenzene (TMB) as the swelling agent to explore the effect of pore size on final adsorbent properties. The pore expanded MCM-41 was also grafted with (3-Aminopropyl)triethoxysilane (APTES) to determine the optimal pore size for $CO_2$ adsorption. The pore-expanded mesoporous MCM-41s showed relatively less structural regularity but significant increments of pore diameter (4.64 to 7.50 nm); the fraction of mesopore volume also illustrated an increase. The adsorption heat values were correlated with the order of the adsorption capacities for pore expanded MCM-41s. After amine functionalization, the adsorption capacities and heat values showed a significant increase. APTES-grafted pore-expanded MCM-41s depicted a high potential for $CO_2$ capture regardless of the major drawback of the high energy required for regeneration.

## 1. Introduction

Fossil fuels will remain in abundant provision well into the 21st century and contribute to the high standard of living enjoyed by the industrialized world. However, the environmental and economic threats caused by possible climate change which is commonly referred to as the greenhouse effect make their future uncertain [1]. In order to reduce global warming and enjoy the benefits of fossil fuels, $CO_2$ adsorption and separation in a cost-effective and environmentally friendly way is one of the most promising means [2, 3].

Several groups [4–9] proposed to immobilize amines onto the mesoporous materials to capture $CO_2$. Mesoporous silica such as MCM [9], SBA [10, 11], MSU [12], silica foam [13], and KIT-6 [14] types have attracted great attention of a large community of researchers for gas separation applications. They found that the $CO_2$ adsorption rate and capacity are chiefly determined on not only amine content but also the support porosity. Moreover, the two factors are not thoroughly independent since supports with higher pore sizes could load more amines. Among many well-known mesoporous materials, MCM-41 offers many advantages in terms of rapid adsorption kinetics, easy-to-design pore structure, large surface area, and low energy required for regeneration [15–17]. Additionally, MCM-41 possesses a large amount of Si-OH on its surface which provides abundant reaction sites and Si in the framework of silica could be replaced by other atoms, which makes the modification easier [18].

Various methods have been developed for the synthesis of MCM-41 silica with larger pore sizes [19–22]. Conventional MCM-41 silica exhibits a typical pore size within the range of 3 to 4 nm. Corma et al. [23] obtained MCM-41 with the pore size of 6 nm to 7 nm after rising the synthesis temperature (408–448 K). Zhao et al. [24] also concluded that the temperature could affect the pore size. Wang and Kabe [25] modified the pH to increase the pore size from 3.83 nm to 5.27 nm. Expanders (e.g., alkanes [26], amines [22], and trimethylbenzene [27]) also have been used for the pore expansion of mesoporous materials. Wang and Yang [10] expanded the pore diameter of SBA-15 through adding TMB

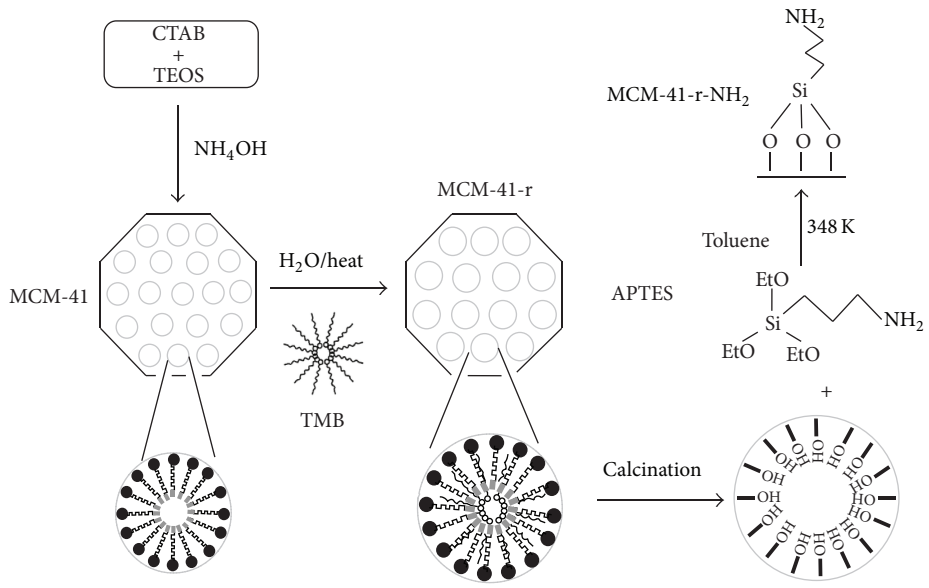


Figure 1: Synthesis route of APTES grafted pore-expanded MCM-41.

as swelling agent to 7.6 nm and after amine grafted, the pore diameter reduced to 5.3 nm. The $CO_2$ adsorption capacity of APTES grafted SBA-15 reached 1.6 mmol/g. Loganathan et al. [19, 28] prepared pore expanded MCM-41 by varying the amount of ammonia (the required preparation materials). As the amount of ammonia decreased, the pore size and volume of MCM-41 increased. The $CO_2$ capacity of pore expanded MCM-41 was as much as 1.2 mmol/g. However, valuable information obtained shows that pore expansion easily led to a decrease of the mesostructure order. When the pore size is larger than 5 nm, the nanostructures become unstable and the pore walls cannot support three-dimensional skeleton; it is likely to cause the structural collapse. The difficulty to modify the pores increases with the presence of swelling agent. Additionally, most papers only found that pore enlargement could enhance the $CO_2$ adsorption performance [4, 22, 29, 30], but few work study the relationship between the pore size and $CO_2$ adsorption behavior.

Therefore, evaluating the optimal pore size is of great importance to synthesis amine-functionalization adsorbents for improved $CO_2$ adsorption. According to this, in this paper, a series of pore-expanded MCM-41s with increasing pore size were used as supports and APTES which contains three amine groups per organic chain was preferred as the grafted species to obtain superior capacity. Well-uniformed pore-expanded MCM-41s were examined; the effect of pore size on $CO_2$ adsorption capacity, surface grafted, and adsorption heat was also investigated.

## 2. Materials and Method

*2.1. Materials.* The reagents of Tetraethylorthosilicate (TEOS) used for the synthesis of pore-expanded MCM41 was purchased from Tianjin Fu Chen Chemical Reagents Factory; the chemical formula is $C_8H_{20}O_4Si$ and the molar mass is 208.33 g/mol, AR. Hexadecyltrimethyl ammonium bromide (CTAB) with the molar mass of 364.446 g/mol was used as the template agent and the chemical formula is $C_{19}H_{42}BrN$. 1,3,5-trimethylbenzene (TMB) was chosen as the swelling agent and produced by Tianjin Guangfu Fine Chemical Research Institute, AR. Ethanol (95% ACS grade), toluene (99% ACS grade), and ammonia (25% ACS grade) were bought from Beijing Chemical Works. (3-Aminopropyl)triethoxysilane (APTES) obtained from J&K Scientific Ltd. was used as the amino silane coupling agent.

Figure 1 illustrates the procedure for the synthesis of pore-expanded MCM-41 and a schematic diagram of the amine grafting. The periodic mesoporous MCM-41 was prepared in the presence of CTAB and TEOS according to the procedure reported by Cai et al. [17] and was further expanded through adding swelling agent. MCM-41-r0, MCM-41-r2, MCM-41-r4, MCM-41-r6, and MCM-41-r8 were successfully synthesized and r means the molar ratio between swelling agent and template agent.

The five pore-expanded MCM-41s were used as supports and APTES was chosen as the amine base to synthesize the amine grafted MCM-41s. Toluene was added to the flask as the reaction solvent, and then excess APTES was added; thereafter, measured MCM-41 was put into the flask; the mixed solution was placed in a magnetic stirrer at 348 K for 20 hours. After cooling the solution to room temperature, the product was recovered by filtration on a Buchner funnel, washed with water, and dried in air at ambient temperature to acquire the amine-grafted materials. The materials were named as MCM-41-r-$NH_2$ s.

*2.2. Characterization and $CO_2$ Adsorption Measurements.* The crystal structures of all adsorbents were characterized by X-ray diffraction (XRD) on D8 ADVANCE (Bruker,

German) diffractometer operating at 40 kV and 30 mA with CuK$\alpha$ radiation (0.1541 nm). The XRD diffraction patterns were taken in the $2\theta$ range of 1.3°–10° at a scan speed of $0.5^\circ \cdot \text{min}^{-1}$.

Pore diameter, volume, and surface area of the samples synthesized were evaluated via $N_2$ physical adsorption analysis through ASAP2020 (Micromeritics, USA) automatic adsorption system. The $N_2$ adsorption data was recorded at the liquid $N_2$ temperature (77 K). The surface area and the pore size distribution were calculated by the BET and BJH equations. The total pore volume was estimated from the amount of adsorbed $N_2$ at the partial pressure $P/P_0 = 0.99$.

Thermal gravimetric analysis (TA Instruments, USA) was applied to determine the amount of amine loading and the thermal stability of adsorbent. From a series of experiments, it was determined to treat the materials at 373 K for a period of 60 min in $N_2$ to remove all the water and $CO_2$ adsorbed from the air. After the initial heat treatment, a heating rate of $10\ \text{K} \cdot \text{min}^{-1}$ up to 973 K in $N_2$ was conducted to calculate the real amine impregnated on subtracts.

$CO_2$ adsorption measurements were also performed on thermal gravimetric analysis under atmosphere pressure. A mixture gas of 10% $CO_2$ and 90% $N_2$ was used as the model flue gas. In each run, the adsorbents were loaded into an alumina sample pan and afterward pretreated at 283 K for 1 hour in $N_2$ to remove the adsorbed moisture, and then the adsorbents were cooled to the adsorption temperature of 308 K prior to their exposure to the mixture gas. The desorption run was conducted in a pure $N_2$ flow at 373 K to achieve complete desorption.

## 3. Results and Discussion

*3.1. Material Characterization.* The Nitrogen adsorption isotherms observed from Figure 2 of MCM-41-r0 and MCM-41-r2 exhibit a typical type IV adsorption-desorption isotherm according to the IUPAC classification, which demonstrates the characteristic of mesoporous materials. The capillary condensation in mesopores of MCM-41-r2 in mesopores occurred at a higher relative pressure due to their larger pore diameter compared with conventional MCM-41. The pore diameter of MCM-41-r2 increased significantly to 5.12 nm. The pore volume of MCM-41-r2 was around $1.00\ \text{cm}^3$, similar to the value of MCM-41-r0. The pore-expanded MCM-41-r2 showed comparably lower pore volume of $771\ \text{m}^2/\text{g}$ but the value is not far from that of conventional MCM-41 ($865\ \text{m}^2/\text{g}$). The pore size of MCM-41-r2 increased significantly but the mesostructure order decreased as a result of pore expansion. In order to continuously enlarge the pore size of MCM-41, more swelling agent was required to add into the mixture; however, excessive swelling agent may destroy the mesostructure.

Due to a slight loss of the mesostructure during the pore-expansion process, the intensity of diffraction peaks of MCM-41-r2 was lower than that of MCM-41-r0 [31] as demonstrated in Figure 3 which showed the XRD patterns of MCM-41-r0 and MCM-41-r2. The highest peaks observed shifted to lower

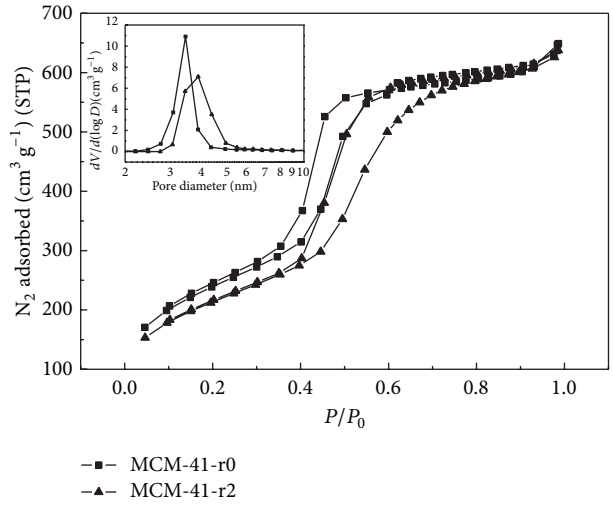


Figure 2: The Nitrogen adsorption isotherms of MCM-41-r0 and MCM-41-r2 and the distribution of pore size.

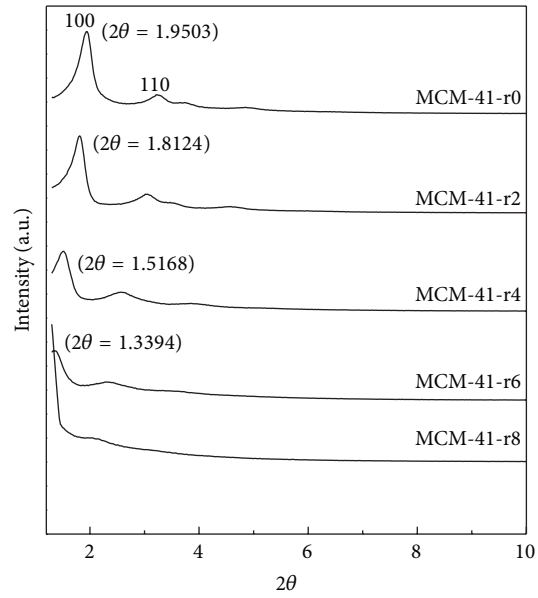


Figure 3: The XRD patterns of pore-expanded MCM-41s.

$2\theta$ from 1.9503° to 1.8124°, and the smaller $2\theta$ related to the large cell parameters.

As shown in Figure 3, all the pore-expanded MCM-41s were studied to explore the effect of swelling agent on structure characteristics. In the process of pore-expanding, when increasing the amount of TMB, TMB molecules congregate to form "big oil particle" and TMB added to the reaction gel can be solubilized inside the hydrophobic regions of micelles. The hydrophobic solvate interaction of the aromatic molecule with the hydrocarbon tails is analogous to the hydrophilic solvate interaction of water with the charged head groups of CTAB. This caused an increase in the micelle diameter and an enlargement of the pore size. The TMB between the surfactant molecules of the micelles can interact with

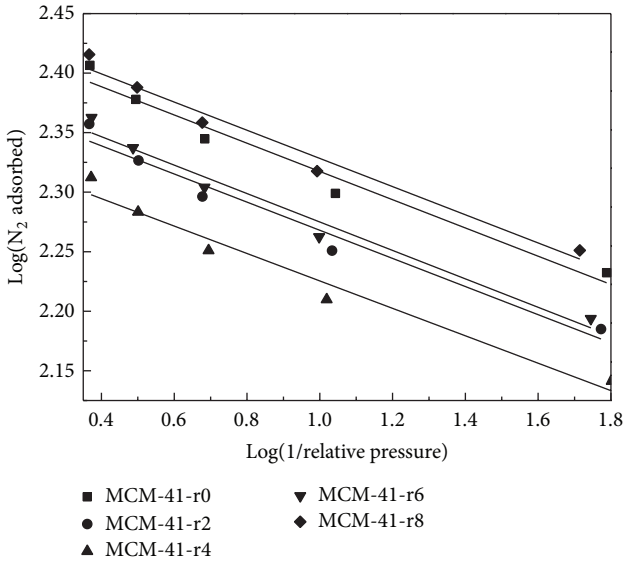


Figure 4: D-R plots of $N_2$ adsorption isotherm on the pore expanded MCM-41.

the ammonium cations of the surfactants through its $\pi$-electrons. It caused an additional increase in the micelles and consequently an enlargement of the pore size [32]. It is clear that the peaks between 1° and 2° can still be observed when the ratios of TMB/CTAB are less than 8; however, the intensity of the peaks decreased greatly. The pattern had a clear (100) peak at 1.9503°; the sample prepared using a TMB/CTAB ratio of 2 exhibited a d(100) spacing of 5.12 nm compared with 4.64 nm in the absence of TMB. No peak was detected for samples synthesized with the TMB/CTAB ratio of 8, indicating that a disordered pore structure was obtained. From inspection of these XRD patterns, a conclusion is drawn that the structural ordering of the obtained materials decreases as the ratio of TMB/CTAB increases.

Figure 4 depicts the micropore volume of the pore expanded MCM-41 calculated using the Dubinin-Radushkevich (D-R) equation [33]:

$$\log W = \log W_0 - D\left(\log\left(\frac{P}{P_0}\right)\right)^2. \quad (1)$$

Here, $D = B(T/\beta)^2$, $B$ is the adsorbent constant, $\beta$ is the affinity coefficient, $W$ is the amount of the liquid adsorbate at relative pressure of $P/P_0$, and $W_0$ is the micropore volume. The results are shown in Table 1, with the increase of the molar ratio between swelling agent and template agent; both mesopore volume and percentages of mesopore volume were increasing which proved that the pore expanded mesoporous MCM-41s were synthesized successfully.

Table 1 also summarizes the textural properties calculated from $N_2$ adsorption isotherms. As the swelling agent increased, the pore sizes rose slightly from 4.64 nm to 7.50 nm. In the process of crystallization reaction, the TMB molecules entered the surfactant micelles, and, consequently, the pore sizes were expanded. The increase of TMB resulted in the concomitant increase of pore size, but when the amount increased consecutively, the dissolution degrees were inconsistent in the micelle due to the effect of hydrophobic; the structural order of the hexagonal mesophase would be destroyed [30] and foam-like structures would be obtained [34]. The destroyed mesostructure made the change of surface area and pore volume irregular. As a result, the surface area and pore volume showed no significant change. Although calcined MCM-41-r8 showed structural disordering, it exhibited relatively narrow pore size distribution. Therefore, it was suitable to immobilize more APTES inside the pores.

In a further step, MCM-41-r0, MCM-41-r2, MCM-41-r4, MCM-41-r6, and MCM-41-r8 were grafted with APTES to study the effect of amine base on structure. As shown in Figure 5, it depicts the XRD patterns of amine-grafting

Table 1: Pore structure parameters of the MCM-41s used different amount of swelling agent.

| Sample | $S_{BET}$[a] $m^2/g$ | $V_{total}$[b] $cm^3/g$ | $V_{Micro}$[c] $cm^3/g$ | $V_{Meso}$[d] $cm^3/g$ | $F_{meso}$[e] % | $d$[f] nm |
|---|---|---|---|---|---|---|
| MCM-41-r0 | 865 | 1.00 | 0.27 | 0.73 | 0.73 | 4.64 |
| MCM-41-r2 | 771 | 0.98 | 0.24 | 0.74 | 0.76 | 5.12 |
| MCM-41-r4 | 696 | 0.97 | 0.22 | 0.75 | 0.77 | 5.61 |
| MCM-41-r6 | 784 | 1.28 | 0.24 | 1.04 | 0.81 | 6.57 |
| MCM-41-r8 | 780 | 1.61 | 0.28 | 1.33 | 0.83 | 7.50 |

[a]$S_{BET}$: surface area calculated using BET equation.
[b]$V_{total}$: total pore volume estimated at relative pressure.
[c]$V_{Micro}$: micropore volume is determined from the Dubinin-Radushkevich equation.
[d]$V_{Meso}$: subtraction of micropore volume from total volume.
[e]$F_{meso}$: fraction of mesopore volume.
[f]$d$: the average pore diameter.

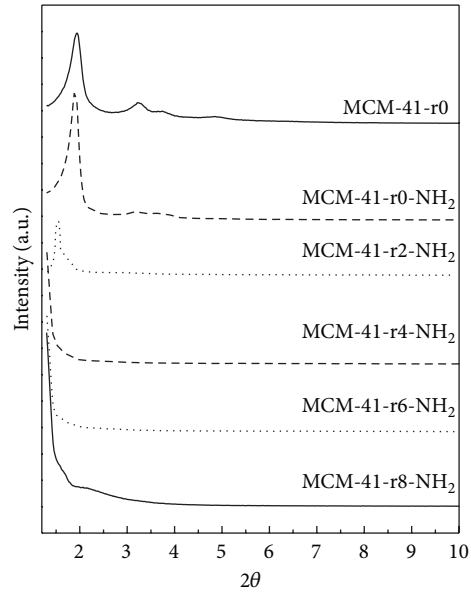


Figure 5: The XRD patterns of amine-grafting pore-expanded MCM-41s.

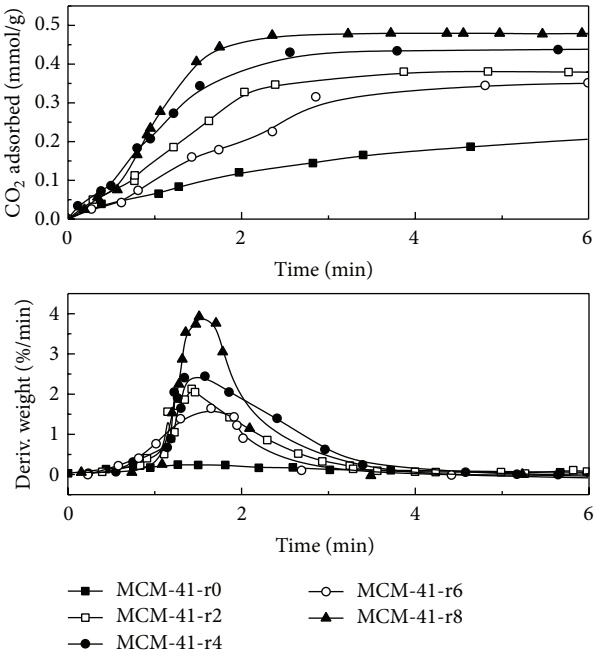


Figure 6: Adsorption curves and adsorption rate curves of pore-expanded MCM-41s.

pore-expanded MCM-41s compared with the original pore-expanded MCM-41; the degree of order of APTES-grafted pore-expanded MCM-41s reduced significantly as a result of grafting. It related to the presence of organosilane molecules within the pores of pore-expanded MCM-41 [31]. For MCM-41-r4-$NH_2$, MCM-41-r6-$NH_2$, and MCM-41-r8-$NH_2$, the mesostructure was not maintained. However, the influence of amine fictionalization and pore size could be concluded by the trend.

### 3.2. Adsorption

*3.2.1. Influence of Pore Size on Adsorption.* Figure 6 shows the $CO_2$ adsorption capacity and the adsorption rate on MCM-41-r0 at 308 K under the mixture gas of 10% $CO_2$/90% $N_2$ at a flow rate of 50 mL/min. Pure Nitrogen flowed through the surface of silica in the first 336 s, giving the background absorbance. Then, 10% of $CO_2$ in Nitrogen was substituted in the flow and adsorbed on the silica surface. The corresponding absorbance increased rapidly to reach a steady state. The maximum capacity of MCM-41-r0 calculated from the figure was 0.27 mmol/g and the largest adsorption rate was 0.30%/min.

Table 2 demonstrates the adsorption capacities and rates of the MCM-41-r samples. As seen from the table, the $CO_2$ adsorption capacity and adsorption rate have been significantly improved with the larger pore size when $r < 4$. In this region, MCM-41-r4 showed the largest adsorption capacity and adsorption rate of 0.44 mmol/g and 2.45%/min, respectively, even when the surface area was the smallest, and they were 1.7 and 7.8 times more than the values of MCM-41-r0. The reasons for this apparent discrepancy were that the

Table 2: The adsorption capacities and rates of pore-expanded MCM-41s.

| Samples | Capacity (mmol/g) | Max adsorption rate (%/min) | Adsorption heat (kJ/mol) |
|---|---|---|---|
| MCM-41-r0 | 0.24 | 0.25 | −15.10 |
| MCM-41-r2 | 0.38 | 2.13 | −21.21 |
| MCM-41-r4 | 0.44 | 2.45 | −24.65 |
| MCM-41-r6 | 0.35 | 1.65 | −20.02 |
| MCM-41-r8 | 0.48 | 3.93 | −26.33 |

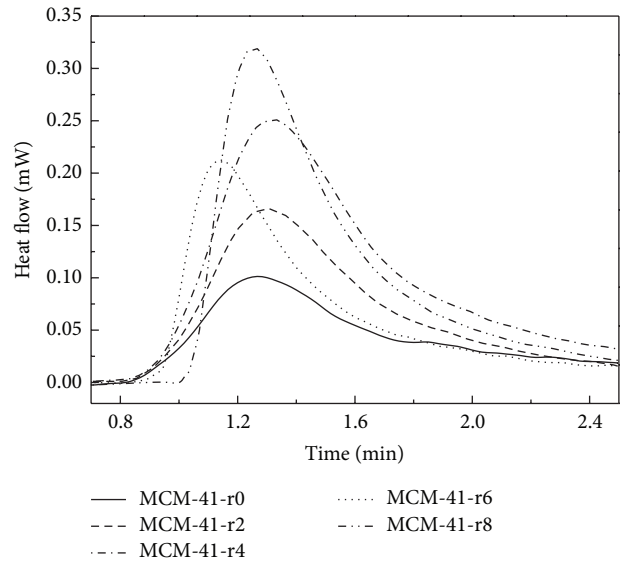


Figure 7: Adsorption heat of pore-expanded MCM-41s.

degree of order and crystallinity still remained high when $r < 4$ although they showed the larger pore sizes. Physical adsorption was enhanced with increasing pore size [31]. However, for MCM-41-r6, the physical adsorption capacity and rate reduced because of the destroyed mesostructure. For MCM-41-r8, the $CO_2$ adsorption capacity and adsorption rate illustrated apparent increases to 0.48 mmol/g and 3.93%/min separately. MCM-41-r8 showed the highest $CO_2$ adsorption capacity and rate, but the mesostructure was totally destroyed; the pore size and characteristics were not uniform; the adsorption mechanism was difficult to distinguish and required further research.

The adsorption heat values of pore-expanded MCM-41 samples are illustrated in Figure 7 and the results are summarized in Table 2. The corresponding values obtained from the thermodynamic analysis increased in the order of MCM-41-r0, MCM-41-r6, MCM-41-r2, MCM-41-r4, and MCM-41-r8 which are correlating with the order of the adsorption capacity; this was also consistent with a higher interaction potential between the adsorbate and adsorbent molecules with larger pore size. MCM-41-r8 showed the highest value of −26.33 kJ/mol. All the values were in the range of −27 to −15 kJ/mol, and it demonstrated that the processes belong to physical adsorption. Weak van der Walls force

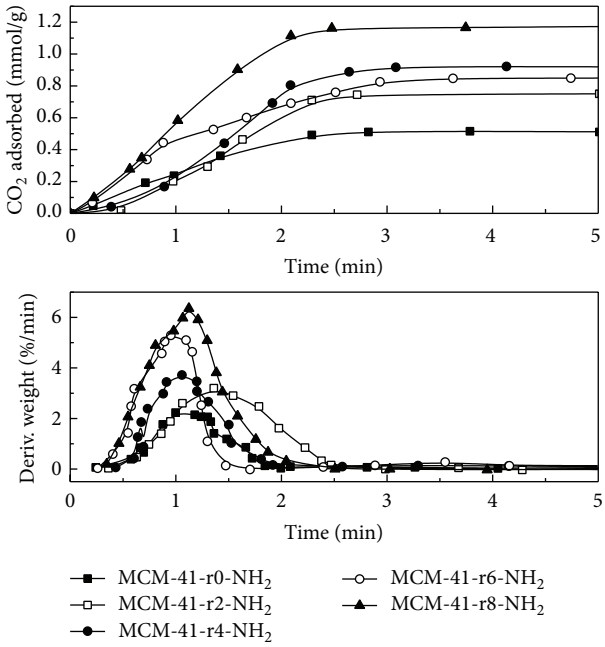


Figure 8: Adsorption curves and adsorption rate curve of pore-expanded MCM-41-$NH_2$.

Table 3: Summary of MCM-41-r-$NH_2$s adsorption data.

| Materials | Adsorption capacity (mmol/g) | Max adsorption rate (%/min) | Adsorption heat (kJ/mol) |
|---|---|---|---|
| MCM-41-r0-$NH_2$ | 0.51 | 1.15 | −45.54 |
| MCM-41-r2-$NH_2$ | 0.74 | 3.36 | −55.46 |
| MCM-41-r4-$NH_2$ | 0.92 | 3.68 | −65.70 |
| MCM-41-r6-$NH_2$ | 0.85 | 3.56 | −60.80 |
| MCM-41-r8-$NH_2$ | 1.16 | 4.28 | −85.79 |

contributed to the adsorption capacity. The negative values of adsorption heat illustrated that the reaction was exothermic between the adsorbent and adsorbate interface.

*3.2.2. Influence of Amine Functionalized to Adsorption.* MCM-41-r-$NH_2$ s were used to study the adsorption performance and calculate the adsorption heat; the adsorbents were kept under the condition of 393 K in the pure Nitrogen for 2 h; after that, switch the gas to 10% $CO_2$/90% $N_2$ for 5 hours to make sure there was no change of the weight.

Figure 8 represents the adsorption and adsorption rate of APTES grafted pore-expanded MCM-41. The maximum capacity calculated from the figure was 1.16 mmol/g and the adsorption heat was −85.79 kJ/mol. The adsorption capacity, adsorption rate, and adsorption heat of other APTES-grafted MCM-41-r samples are exhibited in Table 3. The adsorption capacities of APTES grafted MCM-41 increased significantly due to the amine groups which could react with $CO_2$ molecules. Compared with the original $CO_2$ adsorption capacity of 0.67 mmol/kg, the sample could absorb more

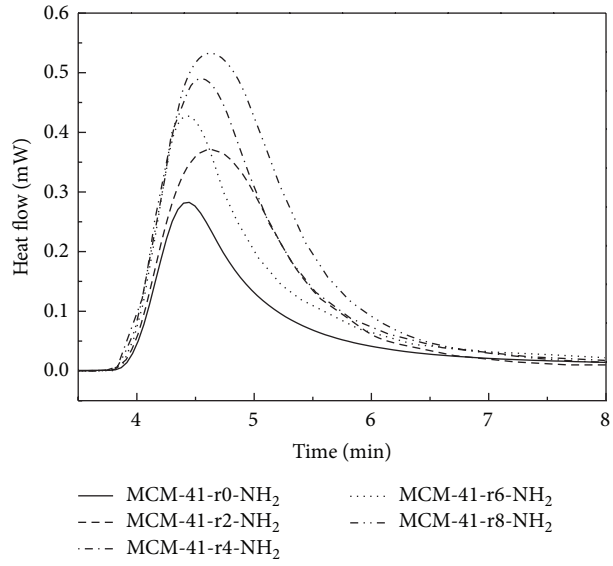


Figure 9: Adsorption heat of APTES grafted pore-expanded MCM-41.

$CO_2$. The adsorption heat values were more than 40 kJ/mol, which indicates the chemical adsorption.

For all amine-grafted materials, APTES grafted pore-expanded MCM-41s exhibited much higher adsorption capacities and adsorption rates than the APTES grafted conventional MCM-41. These data also implied that the pore-expanded MCM-41 material can be grafted with a slightly higher quantity of APTES than the conventional MCM-41. This behavior was largely due to high surface density and the possible aminosilane polymerization at the pore openings. Furthermore, the dynamic adsorption performance of APTES grafted pore-expanded MCM-41s was far superior to APTES grafted MCM-41. The plateau of max adsorption rate (MCM-41-r2-$NH_2$, MCM-41-r4-$NH_2$, and MCM-41-r6-$NH_2$) may be related to the mobility of the $CO_2$ within the pore, caused by the openness of the pore.

Figure 9 and Table 3 depict the adsorption heat of APTES grafted pore-expanded MCM-41; the trend is similar to the adsorption heat of pore expanded MCM-41. From these data, it was apparent that the pore-expanded MCM-41s were capable of grafting more amine but with negative effects of more energy consumption to break the bond between aminosilane and $CO_2$ molecules [35, 36].

The relationship between the fraction of mesopore/micropore volume and the $CO_2$ adsorption capacity of all samples is represented in Figure 10. The $CO_2$ adsorption capacities were increased gradually with the fraction of mesopore volume, whereas the $CO_2$ adsorption capacities of r6 samples were exceptions. The $CO_2$ adsorption capacities likely depend on the fraction of mesopore volume and pore size rather than the surface area and pore volume. The presence of well-developed mesopore is essential for optimum packing of the $CO_2$ molecules at room temperature and pressure. Therefore, a strategy for well-developed mesopore structures and amine functionalization is essential to obtain superior performance for $CO_2$ capture.

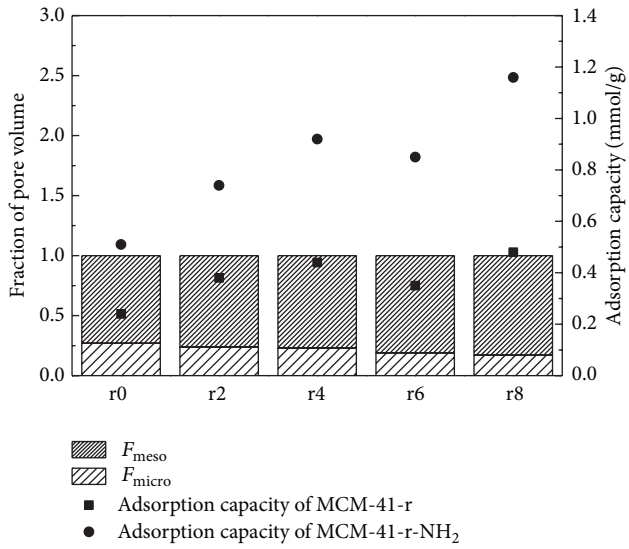


Figure 10: Relationship between the fraction of mesopore/micropore volume and the $CO_2$ adsorption capacity of MCM-41-r and MCM-41-r-$NH_2$.

## 4. Conclusion

Pore-expanded MCM-41s were prepared by 1,3,5-trimethylbenzene as the swelling agent to develop promising large pore $CO_2$ capture adsorbent materials. The design for the pore size was possible by controlling the molar ratio between the swelling agent and template agent. The highest $CO_2$ adsorption capacity for MCM-41-r8 was 0.48 mmol/g which was 1.7 times more than the original MCM-41. In addition, MCM-41-r8-$NH_2$ exhibited the highest adsorption capacity and adsorption rate of 1.16 mmol/g and 4.28%/min, respectively. The adsorption heat values for pore-expanded MCM-41 were in the range of −11.68 and −25.15 kJ/mol. It indicated that the reactions are exothermic and belong to physical adsorption. The adsorption heats of APETS-grafted MCM-41 and pore-expanded MCM-41 were larger than 40 kJ/mol which means chemical adsorption. More energy was needed in the regeneration process to break the bond between aminosilane and $CO_2$ for APTES-grafted pore-expanded MCM-41s since they could not desorb all the $CO_2$ molecules completely. In addition, the $CO_2$ adsorption capacity was strongly affected not by surface area and pore volume but by pore size and mesopore volume fraction. Therefore, modified mesoporous MCM-41 materials with a suitable pore size for $CO_2$ molecules are expected to be excellent solid adsorbents for achieving high $CO_2$ adsorption capacity if regeneration energy requirements could be minimized.

## Conflict of Interests

The authors declare that there is no conflict of interests regarding the publication of this paper.

## Acknowledgments

The authors gratefully acknowledge the National Natural Science Foundation of China (91434120, 51172251), Shanxi Province Coal-based Key Scientific and Technological Project (MD2014-09, MD2014-03), and Fundamental Research Funds for the Central Universities (2014ZD06). Thanks are due to Dr. Kaixi Li for assistance with the experiments and valuable discussion.

## References

[1] A. Somy, M. R. Mehrnia, H. D. Amrei, A. Ghanizadeh, and M. Safari, "Adsorption of carbon dioxide using impregnated activated carbon promoted by Zinc," *International Journal of Greenhouse Gas Control*, vol. 3, no. 3, pp. 249–254, 2009.

[2] T. D. Pham, Q. Liu, and R. F. Lobo, "Carbon dioxide and nitrogen adsorption on cation-exchanged SSZ-13 zeolites," *Langmuir*, vol. 29, no. 2, pp. 832–839, 2013.

[3] C. H. Lee, S. W. Park, and S. S. Kim, "Breakthrough analysis of carbon dioxide adsorption on zeolite synthesized from fly ash," *Korean Journal of Chemical Engineering*, vol. 31, no. 2, pp. 179–187, 2014.

[4] R. S. Franchi, P. J. E. Harlick, and A. Sayari, "Applications of pore-expanded mesoporous silica. 2. Development of a high-capacity, water-tolerant adsorbent for CO2," *Industrial and Engineering Chemistry Research*, vol. 44, no. 21, pp. 8007–8013, 2005.

[5] H. Y. Huang, R. T. Yang, D. Chinn, and C. L. Munson, "Amine-grafted MCM-48 and silica xerogel as superior sorbents for acidic gas removal from natural gas," *Industrial & Engineering Chemistry Research*, vol. 42, no. 12, pp. 2427–2433, 2003.

[6] F. Q. Liu, L. Wang, Z. Huang et al., "Amine-tethered adsorbents based on three-dimensional macroporous silica for $CO_2$ capture from simulated flue gas and air," *ACS Applied Materials & Interfaces*, vol. 6, no. 6, pp. 4371–4381, 2014.

[7] A. Heydari-Gorji, Y. Belmabkhout, and A. Sayari, "Polyethylenimine-impregnated mesoporous silica: effect of amine loading and surface alkyl chains on $CO_2$ adsorption," *Langmuir*, vol. 27, no. 20, pp. 12411–12416, 2011.

[8] A. Boonpoke, S. Chiarakorn, N. Laosiripojana, S. Towprayoon, and A. Chidthaisong, "Investigation of $CO_2$ adsorption by bagasse-based activated carbon," *Korean Journal of Chemical Engineering*, vol. 29, no. 1, pp. 89–94, 2012.

[9] M. Gholami, M. R. Talaie, and S. F. Aghamiri, "Direct synthesis of bi-modal porous structure MCM-41 and its application in $CO_2$ capturing through amine-grafting," *Korean Journal of Chemical Engineering*, vol. 31, no. 2, pp. 322–326, 2014.

[10] L. Wang and R. T. Yang, "Increasing selective $CO_2$ adsorption on amine-grafted SBA-15 by increasing silanol density," *Journal of Physical Chemistry C*, vol. 115, no. 43, pp. 21264–21272, 2011.

[11] N. Gargiulo, A. Peluso, P. Aprea, F. Pepe, and D. Caputo, "$CO_2$ adsorption on polyethylenimine-functionalized SBA-15 mesoporous silica: isotherms and modeling," *Journal of Chemical and Engineering Data*, vol. 59, no. 3, pp. 896–902, 2014.

[12] X. Wang, H. Li, H. Liu, and X. Hou, "AS-synthesized mesoporous silica MSU-1 modified with tetraethylenepentamine for $CO_2$ adsorption," *Microporous and Mesoporous Materials*, vol. 142, no. 2-3, pp. 564–569, 2011.

[13] X. Yan, L. Zhang, Y. Zhang, K. Qiao, Z. Yan, and S. Komarneni, "Amine-modified mesocellular silica foams for $CO_2$ capture," *Chemical Engineering Journal*, vol. 168, no. 2, pp. 918–924, 2011.

[14] R. Kishor and A. K. Ghoshal, "APTES grafted ordered mesoporous silica KIT-6 for $CO_2$ adsorption," *Chemical Engineering Journal*, vol. 262, pp. 882–890, 2015.

[15] X. C. Xu, C. S. Song, J. M. Andresen, B. G. Miller, and A. W. Scaroni, "Novel polyethylenimine-modified mesoporous molecular sieve of MCM-41 type as high-capacity adsorbent for $CO_2$ capture," *Energy and Fuels*, vol. 16, no. 6, pp. 1463–1469, 2002.

[16] A. Samanta, A. Zhao, G. K. Shimizu, P. Sarkar, and R. Gupta, "Post-combustion $CO_2$ capture using solid sorbents: a review," *Industrial & Engineering Chemistry Research*, vol. 51, no. 4, pp. 1438–1463, 2012.

[17] Q. Cai, W. Y. Lin, F. S. Xiao, W. Q. Pang, X. H. Chen, and B. S. Zou, "The preparation of highly ordered MCM-41 with extremely low surfactant concentration," *Microporous and Mesoporous Materials*, vol. 32, no. 1-2, pp. 1–15, 1999.

[18] C. T. Kresge, M. E. Leonowicz, W. J. Roth, J. C. Vartuli, and J. S. Beck, "Ordered mesoporous molecular sieves synthesized by a liquid-crystal template mechanism," *Nature*, vol. 359, no. 6397, pp. 710–712, 1992.

[19] S. Loganathan, M. Tikmani, and A. K. Ghoshal, "Novel pore-expanded MCM-41 for $CO_2$ capture: synthesis and characterization," *Langmuir*, vol. 29, no. 10, pp. 3491–3499, 2013.

[20] D. D. Das, P. J. E. Harlick, and A. Sayari, "Applications of pore-expanded MCM-41 silica: 4. Synthesis of a highly active base catalyst," *Catalysis Communications*, vol. 8, no. 5, pp. 829–833, 2007.

[21] H. M. Zhao, D. Lin, G. Yang, Y. Chun, and Q. H. Xu, "Adsorption capacity of carbon dioxide on amine modified mesoporous materials with larger pore sizes," *Acta Physico-Chimica Sinica*, vol. 28, pp. 985–992, 2012.

[22] A. Sayari, Y. Yang, M. Kruk, and M. Jaroniec, "Expanding the pore size of MCM-41 silicas: use of amines as expanders in direct synthesis and postsynthesis procedures," *Journal of Physical Chemistry B*, vol. 103, no. 18, pp. 3651–3658, 1999.

[23] A. Corma, Q. Kan, M. T. Navarro, J. Pérez-Pariente, and F. Rey, "Synthesis of MCM-41 with different pore diameters without addition of auxiliary organics," *Chemistry of Materials*, vol. 9, no. 10, pp. 2123–2126, 1997.

[24] D. Zhao, Q. Huo, J. Feng, B. F. Chmelka, and G. D. Stucky, "Nonionic triblock and star diblock copolymer and oligomeric sufactant syntheses of highly ordered, hydrothermally stable, mesoporous silica structures," *Journal of the American Chemical Society*, vol. 120, no. 24, pp. 6024–6036, 1998.

[25] A. Wang and T. Kabe, "Fine-tuning of pore size of MCM-41 by adjusting the initial pH of the synthesis mixture," *Chemical Communications*, no. 20, pp. 2067–2068, 1999.

[26] J. L. Blin and B. L. Su, "Tailoring pore size of ordered mesoporous silicas using one or two organic auxiliaries as expanders," *Langmuir*, vol. 18, no. 13, pp. 5303–5308, 2002.

[27] D. M. Jiang, J. S. Gao, J. Yang, W. G. Su, Q. H. Yang, and C. Li, "Mesoporous ethane-silicas functionalized with *trans*-(1*R*,2*R*)-diaminocyclohexane: relation between structure and catalytic properties in asymmetric transfer hydrogenation," *Microporous and Mesoporous Materials*, vol. 105, no. 1-2, pp. 204–210, 2007.

[28] S. Loganathan, M. Tikmani, and A. K. Ghoshal, "Pore-expanded MCM-41 for $CO_2$ adsorption: experimental and isotherm modeling studies," *Chemical Engineering Journal*, vol. 280, pp. 9–17, 2015.

[29] R. Serna-Guerrero, Y. Belmabkhout, and A. Sayari, "Further investigations of $CO_2$ capture using triamine-grafted pore-expanded mesoporous silica," *Chemical Engineering Journal*, vol. 158, no. 3, pp. 513–519, 2010.

[30] S. K. Jana, A. Mochizuki, and S. Namba, "Progress in pore-size control of mesoporous MCM-41 molecular sieve using surfactant having different alkyl chain lengths and various organic auxiliary chemicals," *Catalysis Surveys from Asia*, vol. 8, no. 1, pp. 1–13, 2004.

[31] A. Olea, E. S. Sanz-Pérez, A. Arencibia, R. Sanz, and G. Calleja, "Amino-functionalized pore-expanded SBA-15 for $CO_2$ adsorption," *Adsorption*, vol. 19, no. 2–4, pp. 589–600, 2013.

[32] Q. Wu, F. Zhang, J. Yang, Q. Li, B. Tu, and D. Zhao, "Synthesis of ordered mesoporous alumina with large pore sizes and hierarchical structure," *Microporous and Mesoporous Materials*, vol. 143, no. 2-3, pp. 406–412, 2011.

[33] M. M. Dubinin, "The potential theory of adsorption of gases and vapors for adsorbents with energetically nonuniform surfaces," *Chemical Reviews*, vol. 60, no. 2, pp. 235–241, 1960.

[34] J. S. Lettow, Y. J. Han, P. Schmidt-Winkel et al., "Hexagonal to mesocellular foam phase transition in polymer-templated mesoporous silicas," *Langmuir*, vol. 16, no. 22, pp. 8291–8295, 2000.

[35] M. T. Ho, G. W. Allinson, and D. E. Wiley, "Factors affecting the cost of capture for Australian lignite coal fired power plants," *Energy Procedia*, vol. 1, no. 1, pp. 763–770, 2009.

[36] J. Oexmann and A. Kather, "Post-combustion $CO_2$ capture in coal-fired power plants: comparison of integrated chemical absorption processes with piperazine promoted potassium carbonate and MEA," *Energy Procedia*, vol. 1, no. 1, pp. 799–806, 2009.